Microsc. Microanal. 13, 320–328, 2007
DOI: 10.1017/S1431927607070407

Microscopy AND Microanalysis

© MICROSCOPY SOCIETY OF AMERICA 2007

Error Quantification in Strain Mapping Methods

Elisa Guerrero,[1,*] Pedro Galindo,[1] Andrés Yáñez,[1] Teresa Ben,[2] and Sergio I. Molina[2]

[1]Departamento de Lenguajes y Sistemas Informáticos, CASEM, Universidad de Cádiz, Campus Río San Pedro, s/n, 11510 Puerto Real, Cádiz, Spain
[2]Departamento de Ciencia de los Materiales e I.M. y Q.I., Facultad de Ciencias, Universidad de Cádiz, Campus Río San Pedro, s/n, 11510 Puerto Real, Cádiz, Spain

Abstract: In this article a method for determining errors of the strain values when applying strain mapping techniques has been devised. This methodology starts with the generation of a thickness/defocus series of simulated high-resolution transmission electron microscopy images of $InAs_xP_{1-x}/InP$ heterostructures and the application of geometric phase. To obtain optimal defocusing conditions, a comparison of different defocus values is carried out by the calculation of the strain profile standard deviations among different specimen thicknesses. Finally, based on the analogy of real state strain to a step response, a characterization of strain mapping error near an interface is proposed.

Key words: high resolution transmission electron microscopy, strain mapping, geometric phase analysis, strain distortion quantification, strain profile characterization

Introduction

Recent advances in digital imaging and image-processing techniques, together with improved point-to-point resolution of transmission electron microscopes, have allowed the increasing use of high-resolution transmission electron microscopy (HRTEM) images for the characterization of structure parameters and processes in semiconductor heterostructures at atomic scale.

In particular, during the last decades, extensive research work has been carried out on methods for measuring and mapping displacement fields and strain fields from HRTEM images. Peak finding and geometric phase are the two main approaches for strain mapping; both of them are based on the comparison of the image features with a reference lattice to determine the distortions of the unit cells in the image. The local lattice distortions are then used to obtain the local strain distribution of the crystal.

Peak finding methods (Bierwolf et al., 1993; Bayle et al., 1994; Jouneau et al., 1994; Kilaas et al., 1994; Robertson et al., 1995; Seitz et al., 1998; Kret et al., 2001) work in real space, superimposing a two-dimensional reference lattice extrapolated from a nondistorted region of the material to the experimental one, built up from the set of intensity maxima in the HRTEM image, and calculating the local discrete displacement field at each node. Subsequently, by derivating the calculated displacement field, the strain field is obtained.

Received August 7, 2006; accepted February 28, 2007.
*Corresponding author. E-mail: elisa.guerrero@uca.es

Geometric phase methodology developed by Hÿtch et al. (1998) works in Fourier space, and it consists of filtering the image with an asymmetric filter centered around a Bragg spot in the Fourier transform of a HRTEM lattice image and performing an inverse Fourier transform. The phase component of the resulting complex image gives information about local displacement in a given direction. Local strain field is obtained by derivating the displacement obtained from two noncollinear Fourier components.

Peak finding approaches have some advantages, such as less demanding memory and CPU requirements, given that bidimensional complex Fourier transforms are not needed at all. *Peak pairs* is an alternative algorithm based on the detection of pairs of intensity maxima that improves both the speed of computation and memory requirements, allowing us to analyze HRTEM images of greater size at a lower cost. The peak pairs strain determination algorithm works in real space, and it performs quite well in dislocations (Galindo et al., 2006). On the other hand, *geometric phase* has been shown to be superior to traditional real space algorithms when determining strain mapping in areas containing defects, such as dislocations.

Of primary importance in lattice mismatch strain studies of different heterostructures is the quantification of elastic strains in the vicinity of the internal interfaces; prior knowledge about accuracy and inherent error should be also an important issue in strain mapping.

Different factors can contribute to the inherent strain mapping error and certain requirements for error minimization have been studied (Rosenauer et al., 1996; Kret et al., 1999; Tillmann et al., 2000). Hÿtch and Plamann (2001) suggest a set of practical rules for minimizing strain map-

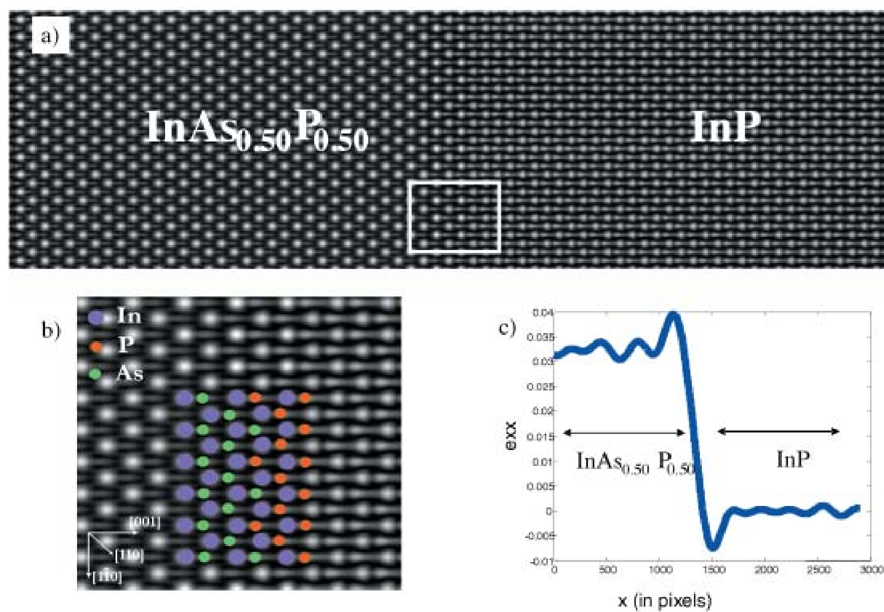

Figure 1. Simulated high-resolution image (1196 × 4096 pixels) of $InAs_{0.50}P_{0.50}$/InP heterostructure (**a**, left and right sides, respectively) for thickness = 12.4 nm and defocus = −61 nm, zoomed interface from the squared area (**b**) and corresponding geometric phase strain profile (**c**).

ping errors, and Rosenauer et al. (2006) demonstrate that artifacts can be kept small for a certain range of specimen orientation and for a large range of defocus values, if a two-beam interference of undiffracted beam and 0002 beam is used, the latter one being aligned parallel to the optical axis. However, to our knowledge, characterization of simulated HRTEM images strain profiles has never been reported in order to quantify systematic error when geometric phase is applied.

Materials and Methods

We analyze the strain distribution near interfaces of $InAs_xP_{1-x}$/InP heterostructures with sphalerite crystalline structure, the electron beam along [110] and for different arsenic contents ($x = 0.25, 0.50, 0.75$) to quantify errors when applying thte geometric phase method. To simulate material diffusion or segregation processes, a linear varying content layer of 1.75 nm has been included at the interface.

A quantification of the intrinsic error has been performed based on the analogy of real state strain to a step response.

First, after the creation of the supercells representing the mentioned heterostructures, a thickness/defocus series of HRTEM images was generated. Simulations were carried out using the EMS software package (Stadelmann, 1987). Electron-optical imaging parameters typical for a JEOL–2011 (accelerating voltage 200 kV, objective lens aperture diameter 9.8 nm^{-1}, aperture shift and origin shift (0,0,0), spherical aberration 1 mm) were used. Beam divergence and defocus spread values have been fixed so as to not add more sources of variation.

A set of 800 images corresponding to 20 different thickness values (from 0.4 nm to 16 nm, steps of 0.8 nm) and 40 different objective lens defocus values (from −80 to −1 nm, in steps of 2 nm) have been generated. Ensuring a high image discretization allows accurate measures of strain; a sampling of 189 picture elements per nanometer has been chosen.

Subsequently, simulated series of images were analyzed using the geometric phase strain mapping method. Experiments were carried out using multiple sets of reflections. Finally, $[\bar{1}11]$ and $[\bar{1}1\bar{1}]$ were selected because smoother phases were obtained.

Figure 1 shows a simulated HRTEM image example of the $InAs_xP_{1-x}$/InP heterostructure for a specific arsenic content of $x = 0.5$ at −61 nm defocus and for a thickness value of 12.4 nm. The strain profile obtained after applying the geometric phase method is shown. A schematic of the model projected interface between alloys is illustrated as an inset on the zoom area.

Lorentzian or Gaussian masks can be used to select the region in reciprocal space to produce the phase images that are sensitive to the precise spacing of the lattice planes (Taraci et al., 2005). During the Fourier filtering, the diameter of the mask applied will determine the effective spatial and spectral resolution and thus, the rippled appearance of the strain profiles. Smoother strain profiles can be obtained by decreasing the width of the region over which the data are averaged; thus we gain spatial information but at the

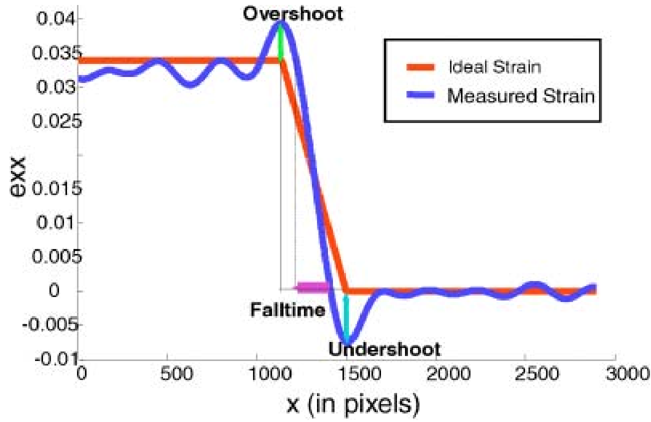

Figure 2. Strain profile measured across the interface InAsP/InP and the characterization parameters of the strain profile.

cost of lost spectral resolution. A compromise between spatial and spectral resolution must be established to obtain reliable strain information. In this work, for the reconstruction of amplitude and geometric phase, a Gaussian mask of ratio g/3 was centred on the Bragg spot **g** in the Fourier space.

The last step of the proposed method consists of optimal defocus determination by strain profile error quantification. Strain profiles are characterized by a sudden jump from the strain value associated with the strained InAsP layer toward the unstrained InP substrate. The theoretical strain profile across an interface can be considered as a smoothed step response, whereas strain profiles from simulated HRTEM images have a rippled appearance that is generated by the sharp edges of the mask in Fourier space (Hÿtch & Plamann, 2001).

In analogy to step characteristics in the signal processing field, three parameters, overshoot, undershoot, and falltime, can be taken into account (Johnson & Graham, 1993). In Figure 2, a graphical description of these parameters is shown.

Overshoot occurs before the transition from a higher to a lower value, when the signal takes a transitory value that is higher than the theoretical strain value. *Undershoot* occurs after the transition from a higher to a lower value, when the output takes a transitory value that is lower than the strain value of the substrate.

Falltime distance represents the interface width of the specimen, due to gradual arsenic content variation from the alloy to the substrate. This parameter states for the minimum layer length that guarantees the appropriate application of any strain mapping method.

Overshoot and undershoot values allow us to gain an insight into oscillations and artifacts that the signal can have, and they could also be related to the falltime parameter. Minimum overshoot and minimum undershoot are desired in order to have a less rippled profile in both sides of the specimen, whereas measured falltime values that are around theoretical interface width are required to minimize the error introduced by strain-distorted areas.

Table 1. Ideal and Determined Strain Values (on Average) at the Strained InAsP Layer for Different Arsenic Contents

Arsenic content	Ideal strain	Average measured strain
25%	0.0171	0.0168
50%	0.0339	0.0324
75%	0.0506	0.0478

Characterization of the averaged strain profiles by means of these parameters allows us to compare strain mapping behavior for different defocus values and to identify the most efficient defocusing conditions.

Real strain values were calculated taking into account the different percentage of composition in the InAsP alloy. The theoretical strain is given by

$$\varepsilon_s = \frac{(a_{\text{epilayer}} - a_{\text{InP}})}{a_{\text{InP}}}. \tag{1}$$

Assuming that the epilayer is a tetragonally distorted pseudomorphic layer, the strain is calculated for [001] as

$$\varepsilon_s = \frac{(a_{\perp} - a_{\text{InP}})}{a_{\text{InP}}} \tag{2}$$

where $a_{\perp}$ corresponds to the $InAs_xP_{1-x}$ lattice distance perpendicular to the (001) and is defined as:

$$a_{\perp} = a_{\text{InP}} + \frac{(1+\upsilon)}{(1-\upsilon)}(a_{\text{InAs}_x\text{P}_{1-x}} - a_{\text{InP}}) \tag{3}$$

- the lattice parameter of the $InAs_xP_{1-x}$ alloy is calculated by Vegard's law:

$$a_{\text{InAs}_x\text{P}_{1-x}} = x\% * a_{\text{InAs}} + (1 - x\%) * a_{\text{InP}} \tag{4}$$

- the bulk lattice parameters of InAs and InP are $a_{\text{InAs}} = 0.60583$ nm and $a_{\text{InP}} = 0.58687$ nm, respectively. Due to the difference between these values, {110} planes for $InAs_xP_{1-x}$ heterostructure grown on InP are stressed and the distance along [001] direction must be elongated.
- Poisson constants for InAs $\nu_{\text{InAs}} = 0.35$ and for InP $\nu_{\text{InP}} = 0.36$.

Results and Discussion

Table 1 shows assumed strain values as well as the strain values determined after applying strain mapping to HRTEM simulated images. The most notable difference between both

sets of strain values is that the maximum amplitude variation and strain measured is slightly lower than expected. This can be attributed to the mask used in Fourier space to calculate the amplitude and phase (Hÿtch et al., 1998).

Figure 3 shows the typical form of the measured strain profile divided into three areas, corresponding to the strained material (A), the strain decreasing interface layer (B), and the unstrained substrate (C).

A first look at strains determined from HRTEM images allows us to observe that, due to the mask effect and windowing functions, areas A and C present oscillations around the $InAs_xP_{1-x}$ strain value and around the zero value of the unstrained InP substrate. Characterization parameters are determined in area B that corresponds to interface strain mapping.

Strain profiles from simulated HRTEM images have a rippled appearance due to windowing effects. A window function is a function that is zero-valued outside of some chosen interval. For instance, a function that is constant inside the interval and zero elsewhere is called a rectangular window, which describes the shape of its graphical representation. When another function, or a signal, is multiplied by a window function, the product is also zero-valued outside the interval (Bergen & Antoniou, 2004). Windowing functions are applied to reduce the effects of the leakage. Leakage amounts to spectral information from an FFT showing up at the wrong frequencies. Leakage cannot be avoided, but by applying windowing functions to data prior to performing an FFT, this effect can be notably reduced at the cost of getting more rippled profiles in areas A and C (Fig. 3). These areas identify the strain value associated with the strained InAsP layer (area A) and the unstrained InP substrate (area C).

Specimen thickness and defocusing conditions have a strong impact on the shape of the obtained profiles. Although prior knowledge about specimen thickness is not always available, optimal defocusing conditions can be stated to aim at obtaining strain profiles that are rather in agreement with the predicting strain state and that have a minimal dependency on specimen thickness.

However, the most efficient defocus values are not intuitively obvious, as they correspond to when the transfer is nearly linear and depend on the image periodicity analyzed (Hÿtch & Plamann, 2001). In this work, a defocus comparison criterion has been established, namely, standard deviations of strain profiles among different specimen thickness values.

Standard deviation for every defocus value measures how spread out the strain profiles are. If strain profiles are all close to the reference profile, then the standard deviation is closer to zero and indicates optimal defocusing conditions to apply geometric phase. If many strain profiles of different specimen thickness values are very different from the reference profile, then the standard deviation is high (further from zero) indicating nonoptimal defocusing conditions to strain mapping.

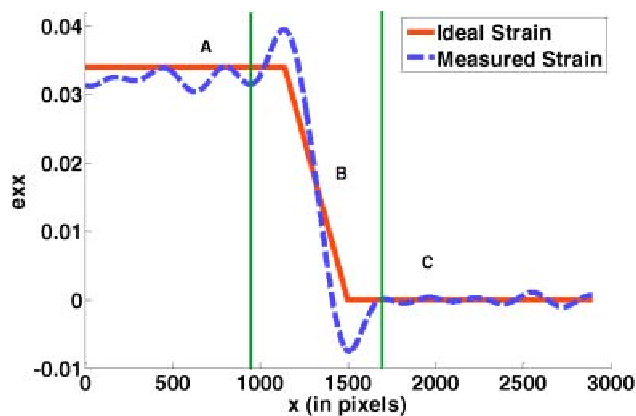

Figure 3. Measured strain profile is divided into three areas to better show the circumstances and reasons for fluctuations and differences from the ideal strain.

Figure 4 shows the standard deviation plots for $InAs_{0.25}P_{0.75}$, $InAs_{0.50}P_{0.50}$, and $InAs_{0.75}P_{0.25}$. The minimum value in each plot is marked, indicating the most efficient defocus value for each composition: −31 nm, −29 nm, and −27 nm, respectively. Notice that the defocus may vary by several nanometers over the field of view of a CCD camera due to specimen-thickness changes and foil inclination. Thus, a range of ±2 nm should be considered.

To further study the optimal defocusing conditions, let us compare a thickness series of simulated HRTEM images for $InAs_{0.50}P_{0.50}$ alloy calculated at optimal defocus (−29 nm) and around Scherzer defocus (−61 nm).

It is important to note that although the results shown from now on are discussed for a 50% percentage of arsenic content, very similar trends are found when investigating other arsenic contents, as can be observed from the figures of strain profiles described below.

By application of geometric phase strain mapping technique, averaged strain profiles are shown in Figures 5–9, where the first row refers to an arsenic content of 25%, the second row to 50%, and third row to 75%.

At the optimal defocus value, increasing strain misfit can be observed as the thickness grows. In contrast, whereas −61 nm defocus, for lower and higher thicknesses, results in profiles that are greatly in agreement with predicting profiles, for intermediate values they very differ from the ideal state. At around Scherzer defocus, averaged strain profiles are strongly distorted for thicknesses ranging from 7.6 to 13.2 nm, showing great fluctuations in both strained and unstrained sides of the profile.

These distortions and differences can be better quantified with the strain profile characterization proposed in this article. Overshoot and undershoot parameters measure maximal difference of measured strain values. These parameters give an insight into the fluctuations of the signal around strain values and should be kept close to zero. Falltime represents a slight overestimate of the interface width, actually amounting to 1.75 nm.

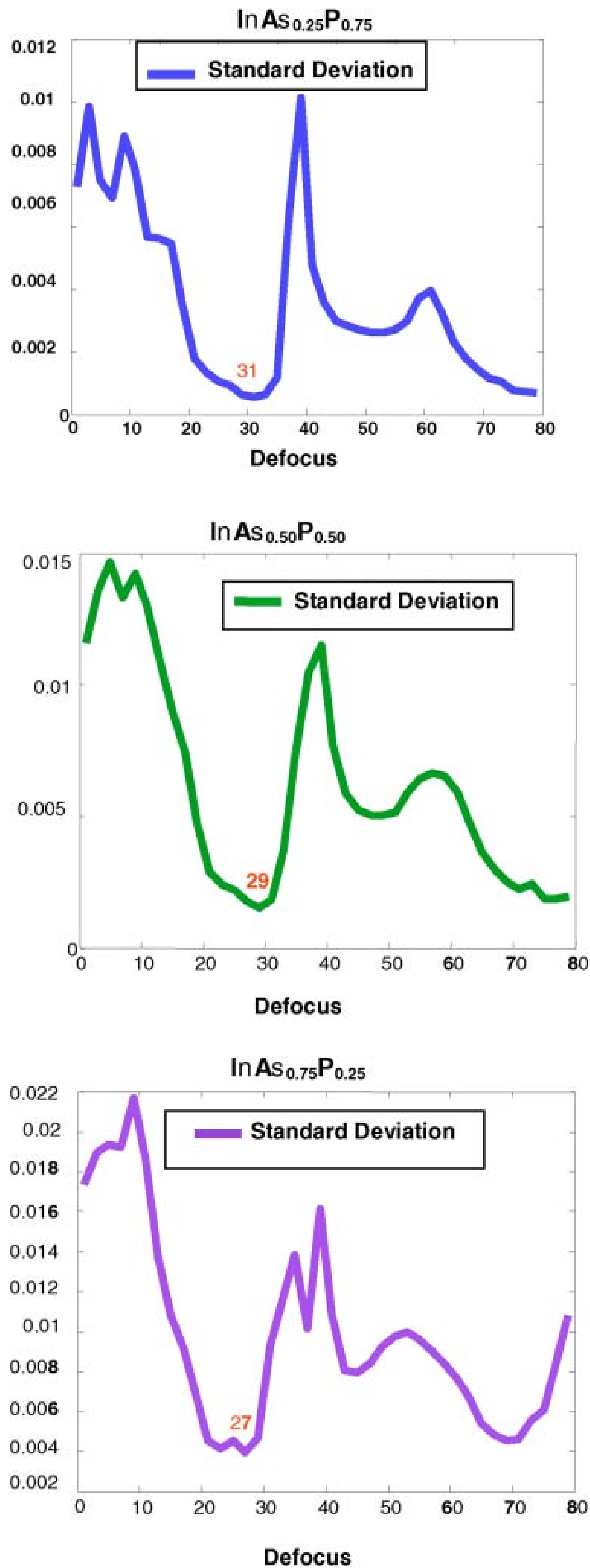

Figure 4. Plots of the standard deviations for $InAs_{0.25}P_{0.75}$, $InAs_{0.50}P_{0.50}$, and $InAs_{0.75}P_{0.25}$; the minimum value in each plot is marked, indicating the most efficient defocus value for each composition: −31, −29, and −27 nm, respectively.

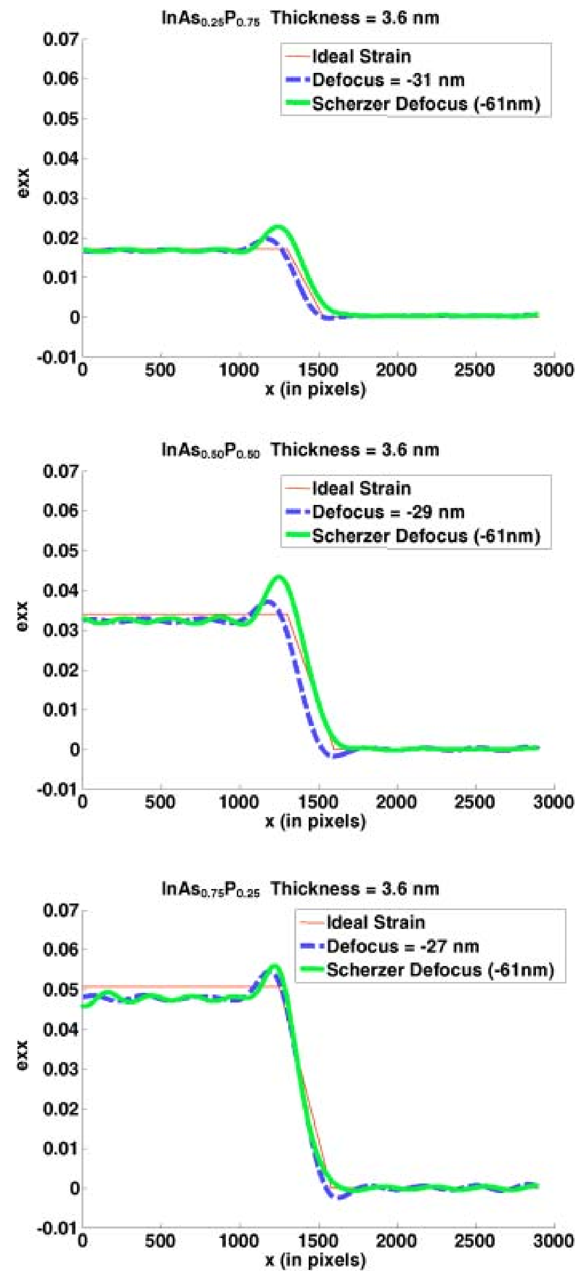

Figure 5. Strain profiles for specimen thickness 3.6 nm considering different arsenic contents: 25%, 50%, and 75%. Optimal defocus remains closer to the real strain state than at the Scherzer defocus.

At around Scherzer defocus, best strain profiles could be identified for specimen thickness from 12.4 to 14 nm (Fig. 9); although overshoot differences are very significant, undershoot and falltime measures represent very low error values.

If heterostructures characterized by a smaller arsenic content are investigated, strain characterization parameters are also smaller, yielding less misfit in the strain profiles. With higher arsenic content, distortions, artifacts, and characterization parameters are also higher. Figure 10 depicts

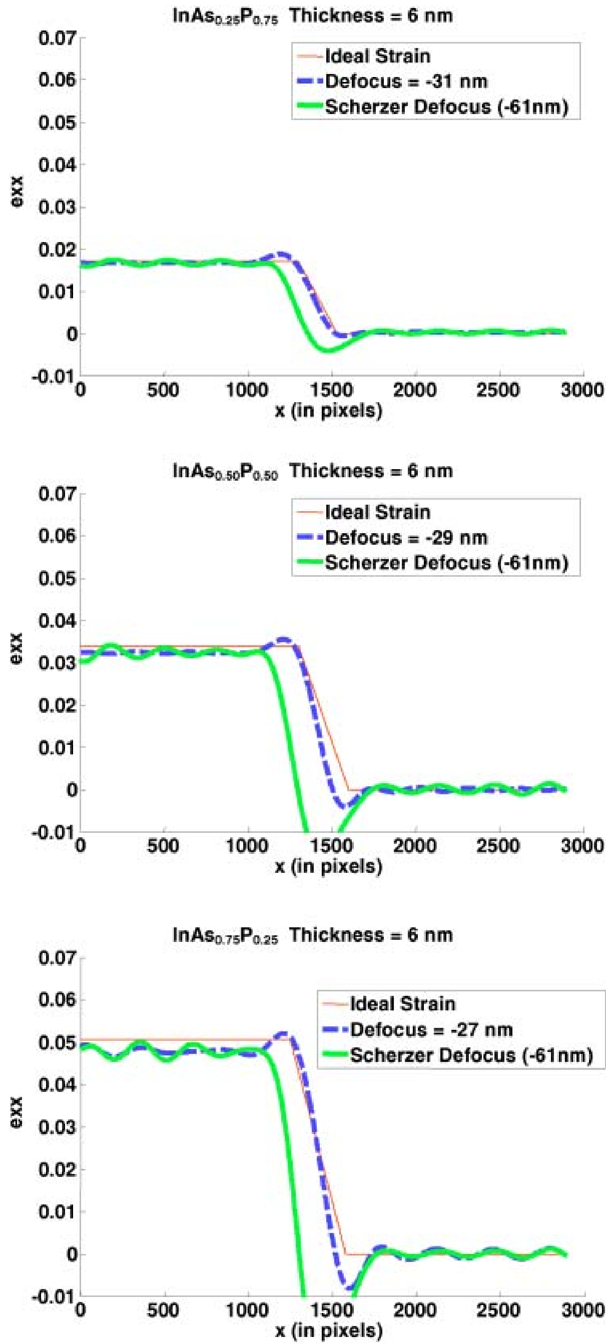

Figure 6. Strain profiles for specimen thickness 6 nm considering different arsenic contents: 25%, 50%, and 75%. Great undershoot misfit appears at −61 nm whereas the optimal defocus remains closer to the real strain state.

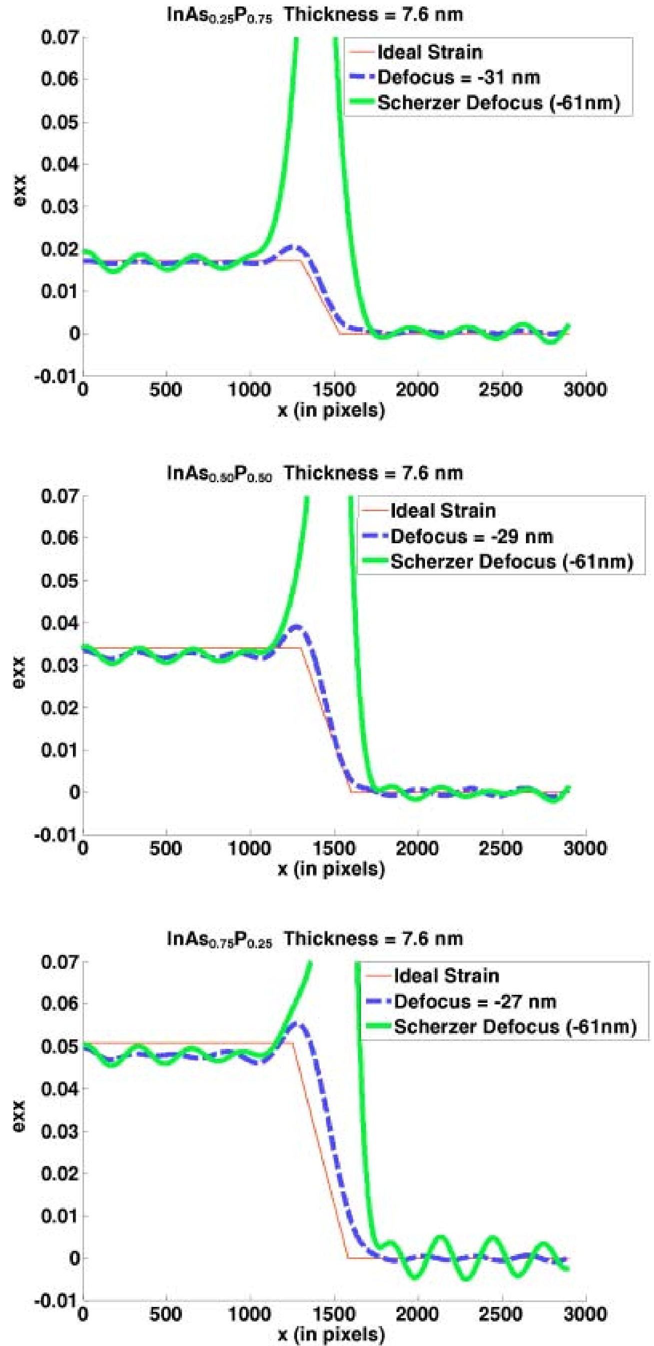

Figure 7. Strain profiles for specimen thickness 7.6 nm considering different arsenic contents: 25%, 50%, and 75%. Great overshoot misfit appears at −61 nm whereas the optimal defocus remains closer to the real strain state.

this effect in the case of the overshoot parameter, at selected and Scherzer defoci. For the different arsenic contents, differences are higher as the arsenic content grows.

Figure 11 shows overshoot plots; at optimal defocus, deviations go up to thicker specimens, whereas at around Scherzer defocus and intermediate thickness values ranging from 6.8 to 11.6 nm, overshoot values illustrate the great distortions presented in the strain profiles.

Figure 12 shows plots for undershoot measures. Undershoot distances decrease, that is, they are closer to zero values, with increasing thicknesses. At Scherzer defocus, undershoot values are closer to zero for very thin specimens; more fluctuations are observed at intermediate thickness values and go closer to zero from 12.4 to 15.6 nm.

Falltime error plots are shown in Figure 13. Although for specific thicknesses, falltime error might seem lower at

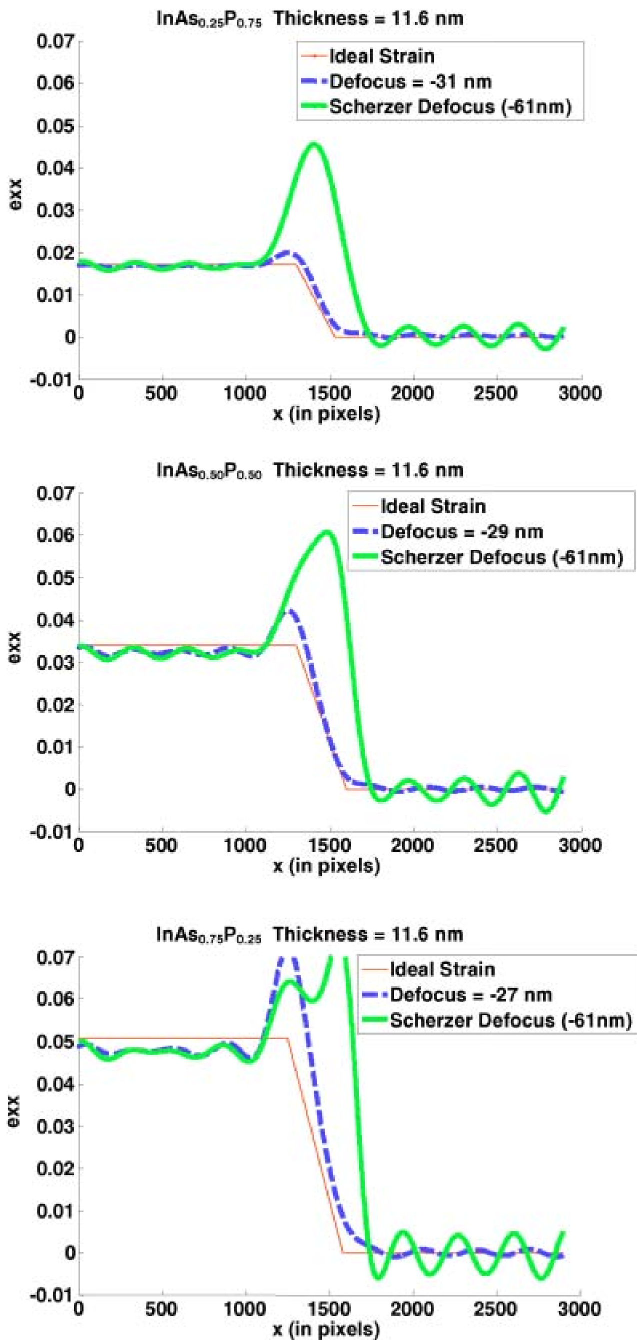

Figure 8. Strain profiles for specimen thickness 11.6 nm considering different arsenic contents: 25%, 50%, and 75%. Great overshoot misfit appears at −61 nm whereas the optimal defocus remains closer to the real strain state.

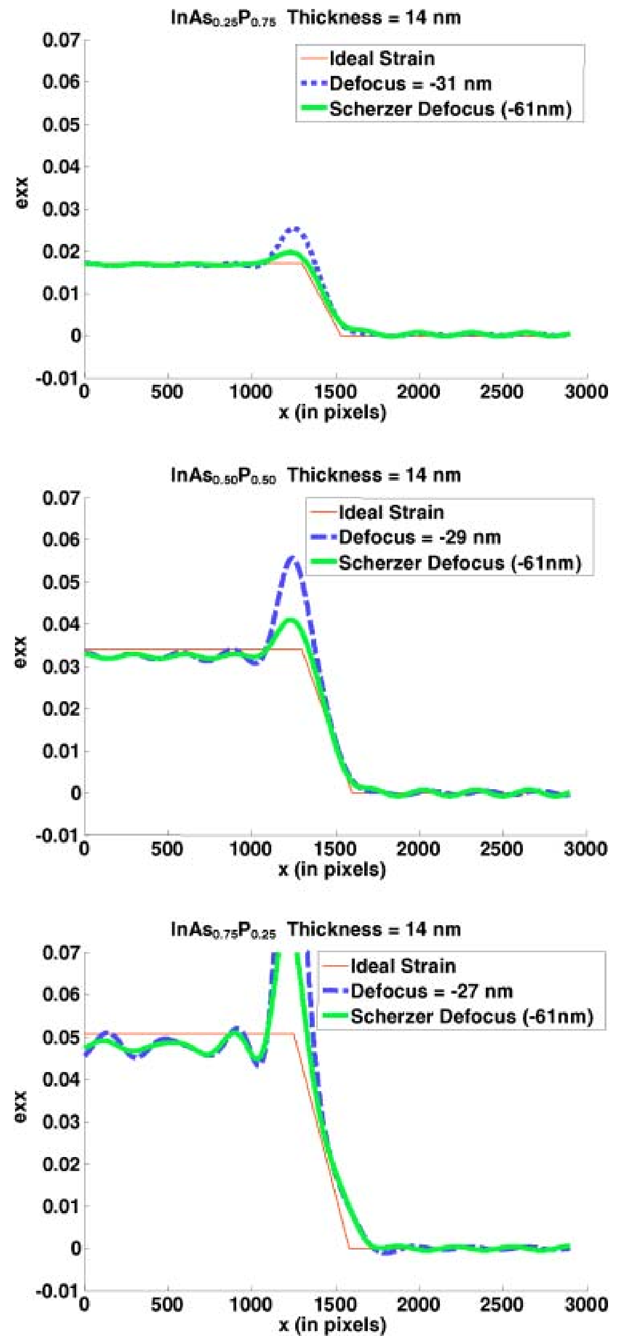

Figure 9. Strain profiles for specimen thickness 14.0 nm considering different arsenic contents: 25%, 50%, and 75%. This is a case where the Scherzer defocus appears to be better than the proposed optimal defocus.

−61 nm than at −29 nm, average falltime over the thickness series amounts to 0.39 nm at optimal defocus, whereas at around Scherzer defocus it amounts to 0.86 nm.

Notice that, at −61 nm defocus, a very important misfit appears at 6 nm thickness, as can be observed from the strain profiles of Figures 6, 7, and 8 as well as undershoot plots in Figure 12 and falltime plots in Figure 13. For next thicknesses up to 10.0 nm, this trend changes and higher overshoot misfit are encountered instead (Fig. 12). This change is not so noticeable looking at falltime plots in Figure 13.

Strain interpretation by means of falltime errors should always be carried out in conjunction with overshoot and undershoot measurements, which give an insight into oscil-

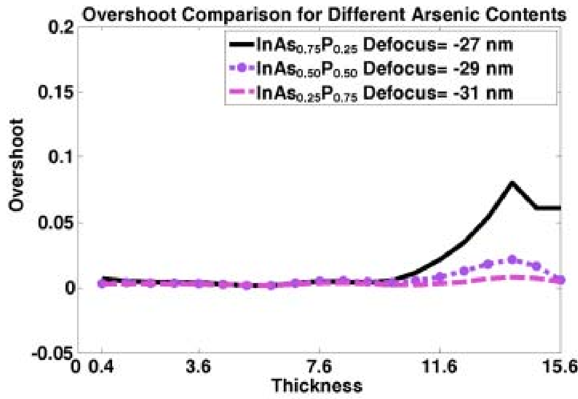

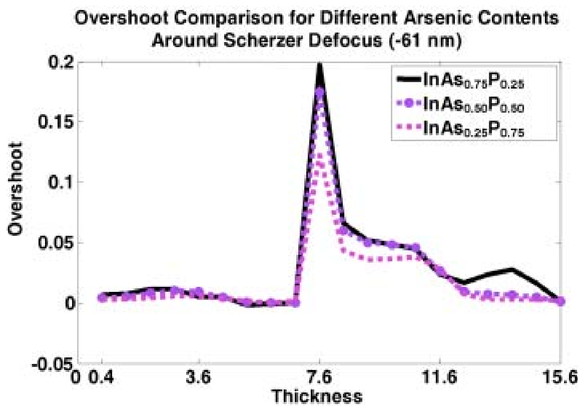

Figure 10. Overshoot comparison (for different arsenic contents) among different thickness values. Overshoot increases with increasing As content. **a**: Comparison at optimal defocus values (−31, −29 and −26 nm for 25%, 50%, and 75% arsenic content, respectively). **b:** Overshoot comparison at the Scherzer defocus (−61 nm).

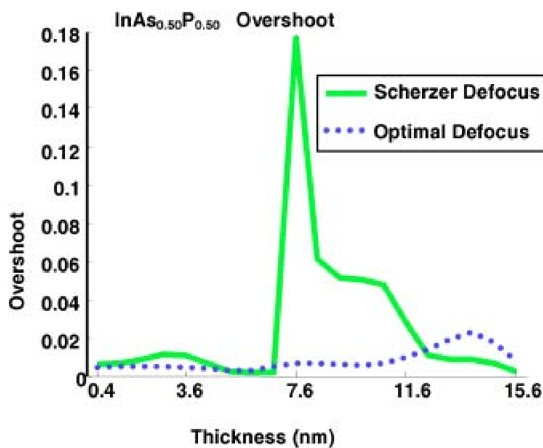

Figure 11. Overshoot plots for $InAs_{0.50}P_{0.50}$, at the optimal defocus value of −29 nm and around the Scherzer defocus, namely, −61 nm.

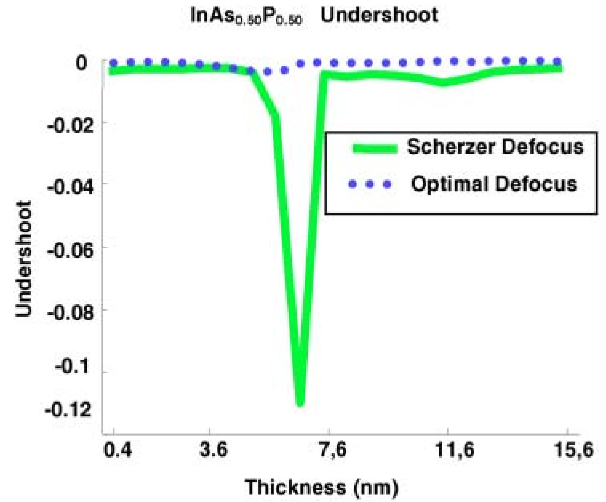

Figure 12. Undershoot plots for $InAs_{0.50}P_{0.50}$, at the optimal defocus value of −29 nm and around the Scherzer defocus.

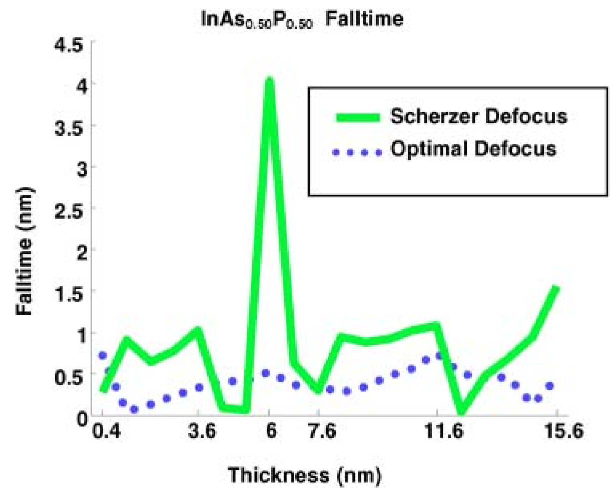

Figure 13. Falltime plots for $InAs_{0.50}P_{0.50}$, at the optimal defocus value of −29 nm and around the Scherzer defocus.

lations in the strained and unstrained sides of the profile near the interface.

Because InP has a noncentrosymmetric structure, errors owing to thickness changes are more likely to occur, as Hÿtch and Plamann (2001) stated.

Conclusions

In this work, a procedure for characterization of strain profiles obtained after applying strain mapping to HRTEM images is proposed. To illustrate our proposal, we use InAsP for different arsenic contents. The shapes of the measured

lattice strain profiles may contain severe artifacts for different thickness and defocus values; however, a systematic error dependent on these features has not been identified. In analogy to frequency responses in the signal processing field, the theoretical strain profile across an interface can be considered as a step response. Most applications of these rapidly changing outputs require minimal fluctuations in the initial state as well as fast settling time in the ideal state. Such requirements can be measured using three important parameters of the signal: falltime, overshoot, and undershoot. Precise determination of such parameters in simulated HRTEM images allows us to numerically quantify lower boundaries of the inherent strain mapping error as well as defocus conditions comparison.

Some general guidelines for applying the proposed methodology can be established:

- When applying geometric phase, an appropriate diameter mask has to be determined to keep the trade-off between spatial and spectral resolution.
- Minimum values of overshoot and undershoot are desired in order to have a less rippled profile in both sides of the strain representation.
- On the other hand, measured falltime values that are around theoretical interface width are required in order to minimize the error introduced by strain-distorted areas.
- Strain interpretation by means of falltime distance should always be carried out in conjunction with overshoot and undershoot measurements, which give an insight into oscillations in the strained and unstrained sides of the profile near the interface.

When a strain mapping technique is applied, default Scherzer defocus choice has been demonstrated to not have to be the optimal one, because a high degree of misfit with respect to the ideal strain state has been observed around this defocus value.

The materials used in the study were InP and $InAs_xP_{1-x}$ for different values of x, but the whole methodology could analogously have been applied to other materials.

Acknowledgments

This work was supported by Spanish MEC under NANOSELF II project (TEC2005-05781-C03-01 and 02/MIC) and by SANDiE European network, Contract NMP4-CT-2004-500101. We also thank the Junta de Andalucía (PAI research groups TIC-145 and TEP-120).

References

Bayle, P., Deutsch, T., Pilles, B., Lancon, F., Marty, A. & Thibault, J. (1994). Quantitative analysis of the deformation and chemical profiles of strained multilayers. *Ultramicroscopy* **56**, 94.

Bergen, S.W.A. & Antoniou, A. (2004). Design of ultraspherical window functions with prescribed spectral characteristics. *EURASIP J Appl Signal Proc* **13**, 2053–2065.

Bierwolf, R., Hohenstein, M., Phillip, F., Brandt, O., Crook, G.E. & Ploog, K. (1993). Direct measurement of local lattice distortions in strained layer structures by HREM. *Ultramicroscopy* **49**, 273–285.

Galindo, P.L., Yañez, A., Pizarro, J., Guerrero, E., Ben, T. & Molina, S.I. (2006). Strain mapping from HRTEM images. In *Microscopy of Semiconducting Materials, Proceedings of the 14th Conference*, April 11–14, 2005, Oxford, UK, Cullis, A.G. & Hutchison, J.L. (Eds.), pp. 191–194. Springer Proceedings in Physics vol. 107. Berlin: Springer.

Hÿtch, M.J. & Plamann, T. (2001). Imaging conditions for reliable measurement of displacement and strain in high-resolution electron microscopy. *Ultramicroscopy* **87**, 199.

Hÿtch, M.J., Snoeck, E. & Kilaas, R. (1998). Quantitative measurement of displacement and strain fields from HREM micrographs. *Ultramicroscopy* **74**, 131.

Johnson, H. & Graham, M. (1993). *High-Speed Digital Design. A Handbook of Black Magic*. Upper Saddle River, NJ: Prentice Hall PTR.

Jouneau, P.H., Tardot, A., Feuillet, B., Mariette, H. & Cibert, J. (1994). Strain mapping of ultrathin epitaxial ZnTe and MnTe layers embedded in CdTe. *Appl Phys* **75**, 7310.

Kilaas, R., Paciornik, S., Schwartz, A.J. & Tanner, L.E. (1994). Quantitative analysis of atomic displacements in HRTEM images. *J Comput Assist Microsc* **6**, 129–138.

Kret, S., Cywiński, G., Wojtowicz, T., Kossut, J., Delamarre, C., Laval, J.Y., Dubon, A. & Chiffmacher, G.S. (1999). Determination of Mn concentration profile in $Cd_xMn_{1-x}Te$ quantum wells with trapezoid confined potential by HRTEM. In *Proceedings of the X Conference on Electron Microscopy of Solids*, Warsaw-Serock, Poland, E. Jezierska & J.A. Kozobowski (Eds.), pp. 167–170. Krakow, Poland: Fotobit.

Kret, S., Ruterana, P., Rosenauer, A. & Gerthsen, D. (2001). Extracting quantitative information from high resolution electron microscopy. *Phys Stat Sol B* **227**, 247–295.

Robertson, M.D., Corbett, J.M., Webb, J.B., Jagger, J. & Currie, J.E. (1995). Elastic strain determination in semiconductor epitaxial layers by HREM. *Micron* **26**, 521.

Rosenauer, A., Gerthsen, D. & Potin, V. (2006). Strain state analysis of InGaN/GaN—Sources of error and optimized imaging conditions. *Phys Stat Sol* **203**, 176–184.

Rosenauer, A., Kaiser, T., Reisinger, J., Zweck, W., Gebhardt, W. & Gerthsen, D. (1996). Digital analysis of high-resolution transmission electron microscopy lattice images. *Optik* **102**, 63.

Seitz, H., Ahlborn, K., Seibt, M. & Schroter, W. (1998). Determination of elastic strains in epitaxial layers by HREM. *J Microsc* **190**, 184–189.

Stadelmann, P.A. (1987). EMS—A software package for electron diffraction analysis and HREM image simulation in materials science. *Ultramicroscopy* **21**, 131.

Taraci, J.L., Hÿtch, M.J., Clement, T., Peralta, P., McCartney, P., Drucker, J. & Picraux, S.T. (2005). Strain mapping in nanowires. *Nanotechnology* **16**, 2365–2371.

Tillmann, K., Lentzen, M. & Rosenfeld, R. (2000). Impact of column bending in high-resolution transmission electron microscopy on the strain evaluation of GaAs/InAs/GaAs heterostructures. *Ultramicroscopy* **83**, 111.